

Challenges in using an analog uncooled microbolometer thermal camera to measure crop temperature

Krzysztof Kusnierek*, Audun Korsæth

(Bioforsk – Norwegian Institute for Agricultural and Environmental Research, Kapp, N-2849, Norway)

Abstract: It has been long known that thermal imaging may be used to detect stress (e.g. water and nutrient deficiency) in growing crops. Developments in microbolometer thermal cameras, such as the introduction of imaging arrays that may operate without costly active temperature stabilization, have vitalized the interest in thermal imaging for crop measurements. This study focused on the challenges occurring when temperature stabilization was omitted, including the effects of focal-plane-array (FPA) temperature, camera settings and the environment in which the measurements were performed. Further, the models for providing thermal response from an analog LWIR video signal (typical output from low-cost microbolometer thermal cameras) were designed and tested. Finally, the challenges which typically occur under practical use of thermal imaging of crops were illustrated and discussed, by means of three cereal showcases, including proximal and remotely based (UAV) data acquisition. The results showed that changing FPA temperature greatly affected the measurements, and that wind and irradiance also appeared to affect the temperature dynamics considerably. Further, it is found that adequate settings of camera gain and offset were crucial for obtaining a reliable result. The model which was considered best in terms of transforming video signals into thermal response data included information on camera FPA temperature, and was based on a priori calibrations using a black-body radiation source under controlled conditions. Very good calibration ($r^2 > 0.99$, $RMSE = 0.32^\circ\text{C}$, $n = 96$) was obtained for a target temperature range of 15-35°C, covering typical daytime crop temperatures in the growing season. However, the three showcases illustrated, that under practical conditions, more factors than FPA temperature may need to be corrected for. In conclusion, this study shows that thermal data acquisition by means of an analog, uncooled thermal camera may represent a possible, cost-efficient method for the detection of crop stress, but appropriate corrections of disturbing factors are required in order to obtain sufficient accuracy.

Keywords: analog thermal camera, uncooled microbolometer, canopy temperature, cereals, UAV

DOI: 10.3965/j.ijabe.20140704.007

Citation: Kusnierek K, Korsæth A. Challenges in using an analog uncooled microbolometer thermal camera to measure crop temperature. *Int J Agric & Biol Eng*, 2014; 7(4): 60–74.

1 Introduction

The use of thermal cameras has been reported in a multitude of environmental applications, including vegetation monitoring. Almost three decades ago,

Jackson et al.^[1] reported that thermal imagery may be used for water stress detection due to a temperature rise in stressed vegetation caused by stomatal closure. They introduced an idea to thermally monitor water stress in vegetation, and thereby provide a means for irrigation scheduling, based on an automatic decision support system. The application of thermal imaging for irrigation scheduling has been successful in arid regions where the temperature difference between air and transpiring canopy is high^[2], but the usefulness of this method has also been reported for other climatic regions^[3].

Thermal imagery has been used for estimating plant stomatal conductance^[4,5] and leaf water stress potential^[2].

Received date: 2014-01-07 **Accepted date:** 2014-07-01

Biographies: Audun Korsæth, PhD, Principal Research Scientist, research interests: precision agriculture, multi-sensory approaches, robotics, C- and N-cycling. Email: audun.korsaeth@bioforsk.no.

***Corresponding author:** Krzysztof Kusnierek, PhD, Research Scientist, research interests: precision agriculture, plant and soil remote sensing, robotics, multivariate data analysis. Email: krzysztof.kusnierek@bioforsk.no. Mailing Address: Bioforsk, Kapp, N-2849, Norway. Tel: +47-92012953.

A more large-scale application of thermography was described by Jones et al.^[6], who used LWIR infrared sensing in drought phenotyping of grapevine (*Vitis vinifera* L.) and rice (*Oriza Sativa* L.). Munns et al.^[7] investigated the genetic variation in the stomatal response to water deficit in wheat (*Triticum aestivum* L.) and barley (*Hordeum vulgare* L.) by means of thermal detection, both under controlled environments and in the field.

Thermal imaging has not only been used for canopy screening. As reviewed by Vadivambal and Jayas^[8], thermal imaging in agriculture and the food industry has been used for e.g. detection of pathogens in plants, ice nucleation, determination of fruit yield, as well as quality assessment of several post-harvest operations. An environmental application of thermography has been demonstrated by Johnson et al.^[9] who used canopy temperature measurements to identify sequestered CO₂ leakage.

Microbolometer thermal cameras record the electromagnetic radiation in the long-wave infrared (LWIR) range. Advances in such cameras include imaging arrays that may operate without costly active temperature stabilization^[10]. This reduces not only the cost of the sensor but also its weight, which opens for a range of new applications in vegetation monitoring, including the use of robotized portable measurement platforms such as Unmanned Aerial Vehicles (UAV).

Small scale agricultural and horticultural enterprises tend to look for measurement systems with low investment cost. The low-cost microbolometer thermal cameras are principally designed for thermal imaging only (e.g. [11]), with an analog video stream as output, i.e. without any direct thermographic capability. Instead, these cameras are typically internally calibrated by the manufacturer to produce 8-bit grayscale images conforming to a measured temperature span, controlled by software settings. Custom radiometric calibration of such images is also possible, but this requires a quantitative relationship of the camera radiance (the 8-bit grayscale value in case of the analog video signal) to a radiative source with known temperature. Usually, a blackbody source is used (e.g. [12]), but water represents

a cheaper alternative for temperature calibration^[13]. To obtain a stable relationship between a grayscale pixel-value and a viewed object temperature, manual adjustment of the camera settings is required during the thermal image acquisition.

In addition to camera calibration and adjustment, the focal-plane-array temperature of uncooled thermal cameras also affects their thermal output. Nugent et al.^[14] proposed a robust mathematical method to correct for such an influence. Their model was, however, designed for a digital output from a thermal camera, not an analog signal. To our knowledge, such a data handling scheme has not yet been designed for the analog output from microbolometer thermal cameras.

In this study, the objective was three-fold. Firstly, we focused on the system challenges which occur when temperature stabilization of a thermal camera is omitted (i.e. a microbolometer uncooled thermal camera), including the effects of focal-plane-array (FPA) temperature, warm-up time, camera settings, and the environment in which the measurements are performed. Secondly, we aimed at developing a method which can be used to transform the camera readings from a typical low-cost, uncooled, analog microbolometer camera (8-bit LWIR video signal) into temperature data. Finally, we tested the use of such low-cost thermal data acquisition to detect crop stress under practical conditions, in order to identify possible constraints and solutions. To do so, we selected three showcases: a) proximal indoor (greenhouse) measurements of phosphorus deficiency in barley, and b) proximal and c) remotely based (UAV) outdoor measurements of water deficiency in wheat.

2 Materials and methods

2.1 Thermal camera setup, calibration and data handling

In this study, we used an uncooled microbolometer LWIR camera (TAU 320, FLIR, USA; Figure 1a), from which the 8-bit analog video stream output was analyzed. The pixel resolution of the camera is 324×256 pixels, which is commonly recognized as a medium resolution. The camera is equipped with an internal uniformity correction and internal temperature calibration, but in the basic version of the camera only the temperature at the

four center pixels is available (shown as an image midpoint temperature value, Figure 1c). For the full image frame, however, the generated output is available as grayscale values only. Hence, a custom camera calibration was required. We calibrated the camera using a blackbody radiation source (Isotech 988, Isotech, UK, Figure 1b) with a range from 15°C to 35°C, and with a thermal resolution of 0.01°C. A video frame of the blackbody radiation source heated up to 25°C is given in Figure 1d.

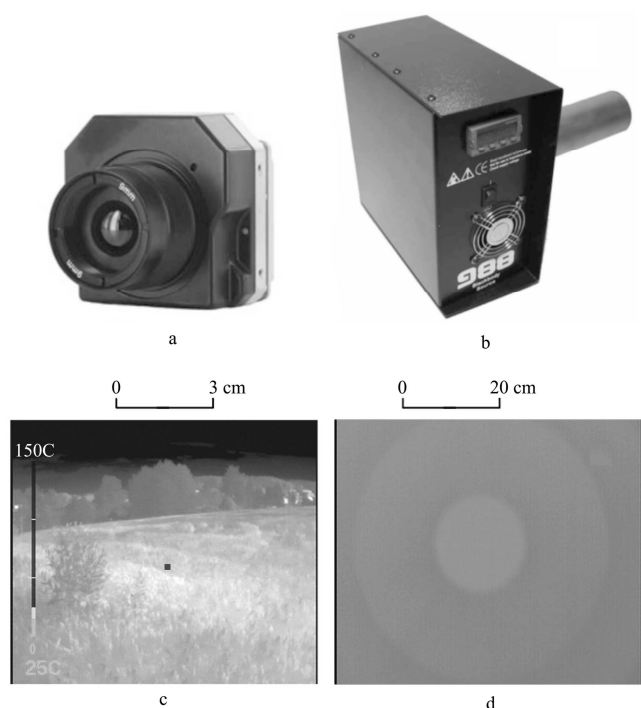


Figure 1 (a) FLIR TAU 320 thermal camera, (b) Isotech 988 blackbody radiation source, (c) thermal image with factory calibrated point thermometer (d) a sample thermal image of a blackbody source at temperature of 25°C (inner circle)

The camera is equipped with automatic adjustment of gain and offset, optimized for thermal detection or identification. To obtain quantitative temperature data, manual settings of these parameters is required (i.e. to maintain the stability and repeatability of the measurements). The optimization of the adequate gain and offset settings is one of the objectives of this work and will be further discussed in the ‘Results and discussion’ section. As a starting point we set the gain value to 25 (in 8-bit scale), and that of offset value to 4500 (in 14-bit scale). It is worth noting, that thermal camera manuals tend to address camera gain and offset as image contrast and brightness, respectively.

The data obtained from digitization of analog video stream using a simple video grabber and video editing software were used in building calibration models. Data handling and calculation procedures were conducted in R^[15] and MATLAB^[16]. In the analysis of the manual setting of the camera the data were interpolated and smoothed using the thin plate splines regression^[17]. In the analysis of the camera initialization time we utilized local polynomial regression fitting^[18] to smooth the experimental data.

2.2 Resolution of the analog video

In this study, we acquired the analog video in Phase Alternating Line (PAL) encoding standard, commonly used to bring high bandwidth, imaging quality and resolution. The analog video was converted into digital (*avi*) format and exported frame-wise as images in high quality *jpg* format. The output resolution of the recorded video stream was 592×512 pixels. In a post processing step we resampled the video images to the actual resolution of the imager (324×256 pixels).

2.3 Geometric calibration

A geometric calibration of the camera is a step required to correct for lens distortion. The wider the field-of-view (FOV) of the lens, the higher the geometric distortion of the image. The calibration procedure detects the intrinsic camera parameter, i.e. focal distance, principal point coordinates as well as lens radial and tangential distortions. Several image calibration methods are available, and we chose to use the Bouguet’s calibration toolbox^[19]. This is a MATLAB procedure designed for semiautomatic extraction of chessboard target corners for visible light imaging cameras. In order to adapt the method to be useable for a thermal camera, we had to make the target thermally recordable. The thermal image calibration literature contains a multitude of possible solutions, including heating a paper chessboard target^[20], building aluminum plates^[21] or designing targets comprised of resistive wires^[22]. We utilized a recently proposed solution of using a checkered cover overlying a heated plate^[23], in our case a monitor display (Figure 2a). The sample raw image used in geometric calibration of the thermal camera procedure and the corresponding corrected image are depicted in

Figures 2b and 2c, respectively.

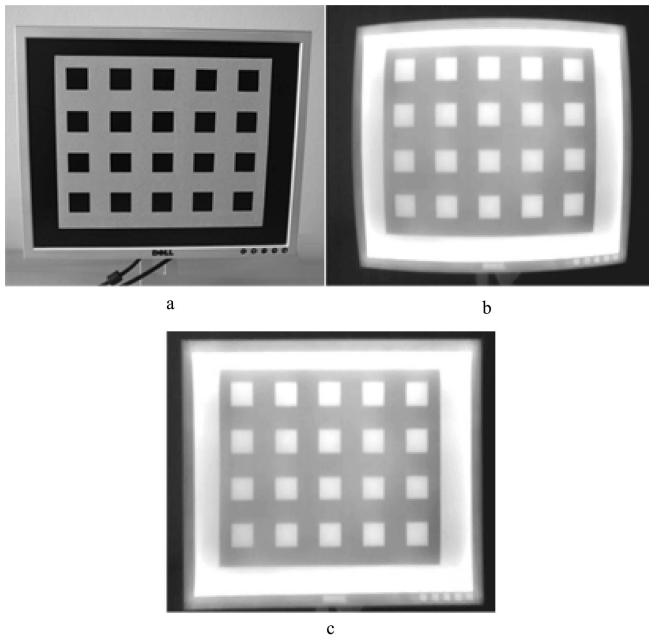


Figure 2 An illustration of the geometric correction (i.e. to correct for lens distortion) using Bouguet's calibration, showing (a) a chessboard target mounted in front of a monitor, (b) a raw thermal image of the setup, and (c) a geometrically corrected thermal image

2.4 Thermal sensitivity

The understanding of the thermal sensitivity of the camera is important in determining the manual gain and offset settings at the analog video acquisition. The relationship between actual thermal sensitivity S_{actual} and f -number f (i.e. focal ratio, which is the ratio of the lens's focal length to the lens diameter) may be expressed by Equation (1)^[24]:

$$S_{actual} = S_{nominal} \times f^2 \quad (1)$$

where, $S_{nominal}$ is the nominal thermal sensitivity of the camera.

Our camera had a nominal thermal sensitivity of 0.05°C , when a lens of $f = 1$ was used. The actual f of our 9mm lens was 1.25. Using Eq. (1), the resulting actual thermal sensitivity of the camera was then $\sim 0.078^{\circ}\text{C}$. This sensitivity applies at a target temperature of 30°C . Thermal sensitivity is, however, also positively correlated with target temperature^[24]. Since the target temperatures measured in this study were somewhat below 30°C , the actual thermal sensitivity of the TAU 320 camera was close to 0.08°C in most cases. Considering the 8-bit data frame of the video signal, the tested camera would thus cover target temperature span of approximately 20°C ($256 \times 0.08^{\circ}\text{C}$).

2.5 Models for transforming analog video signal into thermal response

We considered three alternative strategies for building a model for transforming an analog video signal into thermal response. All strategies involved the use of regression models, and some kind of temperature reference.

In the first approach, FACTORY, we used the image midpoint temperature value, resulting from the factory (i.e. default) calibration of the camera as a reference. A dataset for calibrating a regression model was obtained by sampling several images (covering a range of temperatures). For each image, the pixels closest to the image midpoint were assigned the midpoint temperature value in addition to their original grayscale value (i.e. creating temperature and grayscale value pairs). The temperature values represented the dependent variable in the regression model, whereas the grayscale values were considered as a predictor variable. Additionally, the FPA temperature was recorded at the time when each image was taken, and in some cases used as a second predictor variable.

In a second approach, A PRIORI, calibration data was acquired using laboratory measurements of a blackbody source prior to measurements. Calibration data were obtained at many different FPA levels, by conducting the calibration measurements in rooms with different ambient temperatures.

In the third and final approach, AD HOC, calibration data were acquired using the same blackbody source as for the A PRIORI approach, but the actual calibration was performed in the field before and after the crop monitoring. FPA temperatures were recorded as in the FACTORY approach.

All three approaches followed the same scheme of model building. Initially, linear regression models using grayscale pixel values as the only predictor were fitted to the temperature data. These models were then expanded to include FPA temperature as a second predictor. The next step was to fit quadratic functions to both the single-predictor and the two-predictor (i.e. grayscale value and FPA temperature) data sets. All models were subjected to a leave-one-out cross validation and

evaluated on the basis of their root mean square error (RMSE) and adjusted coefficient of determination (R^2_{adj}), using standard procedures.

2.6 Showcases

Thermal measurements of crops may be of interest both in a greenhouse (indoors) and in the field (outdoors). In the field it is possible to use a thermal camera both as a proximal and as a remote sensor. Various ways of using the camera pose specific challenges in obtaining sound results. We used three experimental showcases to illustrate and discuss challenges, which may typically occur under practical use of thermal imaging of crops: proximal indoor thermal measurement of phosphorus stress in barley, and proximal and remotely based outdoor thermal measurement of water stress in wheat.

2.6.1 Proximal indoor measurement of phosphorus stress in barley

Proximal thermal measurements were performed in a pot experiment conducted in a greenhouse at Bioforsk Arable Crops Department in SE Norway. The pots, which were placed on growing tables at a height of 0.85 m, had a diameter of 0.2 m, each containing 5 liters of soil and 10 growing barley plants. A P stress gradient was obtained by utilizing soil from 15 locations in SE Norway, containing various amounts of plant available P. We utilized only one of the three replicates in the pot experiment, so that our data comprised 15 pots with P-limited barley plants (one from each location) and 15 parallel control pots with barley plants to which an equivalent of 2 g P/m² had been applied to remove any effect of P deficiency, regardless of the initial soil P content. Thermal measurements were performed on 18.03.2013, when the barley plants had reached growing stage BBCH 44. The greenhouse roof ventilation windows were open at the time of the measurement. Each of the 15 pairs comprising P-stressed and control barley plants was imaged from a side view. A uniform background (cardboard) was used to make it easier to extract the plant pixels in the image, needed for the further analyses. The growing tables were distributed evenly throughout the greenhouse, covering 12 m by 5 m. We obtained the ambient temperature gradient by analyzing the temperatures of the cardboard we used as a

uniform background of the images.

To correct for variation in the indoor temperature (see the 'Results and discussion' section), the measured plant temperatures were normalized using the obtained background temperature gradient.

2.6.2 Proximal thermal outdoor measurement of water stress in wheat

For the outdoor showcases we utilized a fertilizer - water stress field experiment in wheat, performed at Yara Research Center in Hanninghof, Germany. The experimental field was divided into a non-irrigated and an irrigated part. The irrigation was performed using a subsoil drip system. Due to the low water-holding capacity of the sandy soil, combined with low precipitation in the time preceding the thermal measurements, the wheat plants in the non-irrigated part showed signs of drought stress. The test field included 36 plots in each water regime (total of 72 plots) and wheat was cultivated under various N fertilization regimes for testing split fertilization rates, which is outside the scope of this study. In the proximal thermal showcase we conducted the measurements on 24 test plots. Weather data were available (minute observations) from a weather station located 200 m from the experimental site.

The proximal measurements were conducted by mounting the camera on a 2 m pole with a 60° off-nadir view zenith angle in order to reduce the influencing in-frame differences of the canopy architecture, and possible effects of bare soil.

Crop growth and status are mainly monitored by means of visible and near-infrared spectroscopy, at midday and with sunny and dry conditions. Thermal measurements, which are generally used for accounting of the water stress in plants^[25], are in practice often conducted in parallel to the spectral acquisition. The measurements conducted at high solar irradiation amplify the temperature differences between stressed and non-stressed plants^[22], but may also be a source of the random variation^[6]. We must consider the anisotropic distribution of the reflective portion of the apparent reflected temperatures measured by the thermal imager. The anisotropic distribution is known as Bi-directional Distribution Function (BRDF), and is related to the view

and solar irradiation horizontal and azimuthal angles. For further reading in this subject, we refer to the work of Snyder et al.^[26]. Although only a few percent of the measured apparent temperature canopy is related to the solar reflectivity, as the emissivity of a healthy crop is at least 0.95^[4,27], its influence on the measured temperature may be high. Regardless of the geometrical correction of the images, conducted in the initial step of the experiment, the radiance distribution in the image is related to the view angles of the camera lens. The relatively low view angle amplifies the differences in solar irradiance distribution. Therefore, to limit this effect, we used only the central area of the images.

2.6.3 Remotely based thermal outdoor measurement of water stress in wheat

We utilized the same field experiment here as for the proximal thermal measurements described in section 2.6.2. The remote measurements were conducted using a Microdrones MD-1000 multi-rotor UAV, operating at a height of 85 m above the ground, with the camera mounted in a nadir view position. In order to reduce the change in FPA temperature and thereby the dependency on the ambient temperature, we introduced a custom camera housing made of a plastic box filled with synthetic foam and covered with a reflective space foil. In the remote thermal showcase we conducted the measurements on 40 test plots.

During processing of the thermal imagery we defined two thermal gradients (see the ‘Results and discussion’ section). To correct for these trends, they were averaged into a general trend, and subsequently subtracted from the dataset.

3 Results and discussion

3.1 System challenges in the absence of temperature stabilization

3.1.1 FPA temperature and warm-up time

It is well known that electromagnetic radiation measurements require a stabilization of the sensor temperature in order to display reliable results (e.g. [22]). Therefore, the first step of the investigation was to test the focal plane array (FPA) temperature after camera initialization and estimate the optimal time for

stabilization of the camera. This was tested under various ambient conditions (Figure 3).

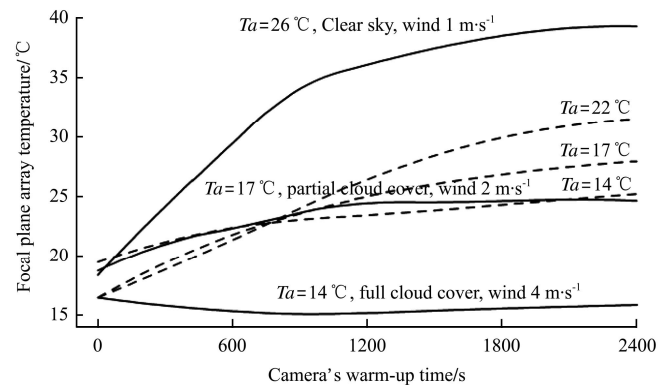


Figure 3 The camera focal-plane-array temperatures (smoothed using local polynomial regression fitting) plotted in the function of time after camera initialization measured indoors (dashed lines) and outdoors (solid lines) at various ambient temperatures (T_a). For the outdoor datasets, observed cloud cover and wind speed, measured at a nearby weather station, are indicated

The time from camera initialization to a relatively stable FPA temperature was highly affected by the ambient conditions (Figure 3). The indoor measurements showed that the time to stabilization increased with increasing ambient temperature. A similar relationship was reported by Berni et al.^[22], who also performed a laboratory experiment on camera warm-up time in their study on remote sensing of vegetation monitoring. The initial change in FPA temperature measured indoors appeared to be at a relatively steady rate. This is probably due to the controlled environment with stable irradiation and high air mass stability. The FPA temperature measured indoors appeared to stabilize after about 30-40 minutes. By comparison, Grant et al.^[27] reported an FPA temperature stabilization time of approx. 10 minutes, when measured under laboratory conditions. The possible reason for their shorter stabilization time could be that they used a different type of camera and/or that the initial camera temperature was higher. The outdoor measurements also revealed a positive correlation between ambient temperature and time until stabilization of FPA temperature (Figure 3). The camera temperature stabilization appeared, however, to be influenced also by wind strength and, to some extent, by the level of radiation related to the type of the cloud cover. Wind

appeared to prevent the camera from warming up to the same extent as in the laboratory, under the same ambient temperature (17°C, Figure 3). In the most extreme case recorded, with wind speed around 4 m/s and ambient temperature of 14°C, the camera warm-up time was only 15-20 minutes.

The temperature of the camera operating outdoors was less stable than indoors. The influence of wind on thermal camera performance has also been reported in other studies. Leinonen et al.^[5] concluded that wind speed had a marked effect on their thermal estimation of stomatal conductance. In a conference paper, Zia et al.^[28] presented results showing a 1.5°C drop in measured temperature when a wind speed of 1.12 m/s was used under laboratory conditions.

The observed effect of lowered radiation due to cloud cover may be explained by the fact that under clear sky conditions the intense direct illumination most likely heats up the camera, while under cloud cover the illumination is more diffuse and does not increase the camera temperature to the same extent.

The outdoor measurements show that the ambient weather conditions may greatly affect the camera

warm-up time and thereby camera stabilization. Measurements performed under changing conditions should therefore be avoided. An uncooled thermal camera should be initialized and exposed to the measuring environment for at least 30-40 minutes before usage.

3.1.2 Manual settings of the camera

The typical analog thermal imager (e.g. a microbolometer camera) is equipped with automatic adjustment of camera gain and offset, optimized for thermal detection or identification. In order to use such an imager to provide quantitative temperature data, manual gain and offset settings are required for retaining stability during measurements. There is a challenge, however, to select a manual setting that returns the desired temperature range with an adequate thermal resolution of the measured scene. To illustrate this, we display (Figure 4) the influence of a camera gain setting (0-255 in 8-bit range) on the grey-scale values recorded by a thermal camera (0-255 in 8-bit range) while observing the blackbody target temperatures between 15 and 35°C. Datasets were sampled at three offset levels (4550, 4700 and 4850 in 4-bit range) and two camera temperature levels (28 and 32.5°C).

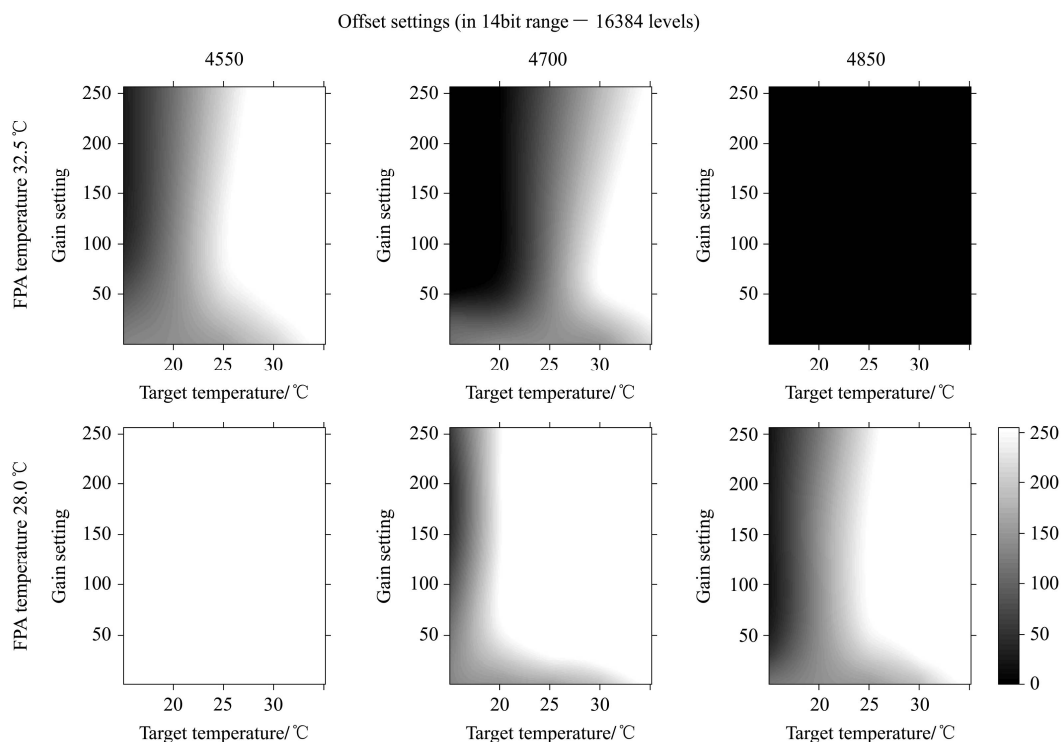


Figure 4 Four major factors influencing a grayscale value of the thermal image illustrated by means of a legend-bar (bottom right), including the temperature of the observed object (abscissa axes), camera gain (ordinate axes), camera offset (values column-wise) and camera's focal-plane-array temperature (values row-wise). The data were interpolated and smoothed using thin plate splines regression

The results showed that the optimum combination of gain and offset settings depended on the FPA temperature. The camera performance was much more sensitive to the offset than to the gain setting. A proper offset setting must be selected at a given camera temperature to match a full 8-bit image dynamic range (i.e.: offset of 4 700 at FPA of 32.5°C). A change in offset from 4 550 to 4 850 (in a 14-bit scale) at a FPA temperature of 32.5°C was, for example, enough to completely level out the measured variation in temperatures (Figure 4, upper left and right sub-plot). The optimum offset appeared to be at 4 700 at the highest FPA temperature (Figure 4, upper left sub-plot), and 4 850 at the lowest temperature measured (Figure 4, lower right sub-plot). At the respective optimum offset level the gain setting could then be used to obtain the best resolution within the temperature span of interest. For example, if we were interested in visualizing the entire target temperature span (15-35°C), the gain should be set very low (below 10 in the 8-bit scale). If a narrower target temperature range as of interest, e.g. 10-15°C, the gain should be set higher (above 50). Using thermal observations for crop monitoring (e.g. plant stress detection), we would normally expect a relatively narrow temperature span. Hence the gain should not be set too low. The thermal sensitivity of the camera is the upper limit of the gain enhancement.

3.2 Empirical model to transform analog thermal video signal into temperature data

We aimed at developing a model which can be used to transform the camera readings from a typical low-cost, uncooled, analog microbolometer camera (8-bit LWIR video signal) into temperature data. Three different strategies of obtaining calibration data were tested, and six different regression models were evaluated within each strategy (Table 1).

The modeling results indicated that the lowest-error modeling strategy (i.e. least RMSE) was to fit a polynomial regression model, including the FPA temperature information, to AD HOC measurements of the calibration blackbody source (around the time of crop monitoring) (Table 1). The AD HOC model was, however, considered to be over-fitted, considering the

low number of calibration points available ($n=11$). In contrast, the approach based on A PRIORI calibration utilized 96 calibration points. The resulting polynomial model, using FPA temperature as an extra predictor, out-performed all the other models (AD HOC models excluded, Table 1).

Table 1 Performance of three alternative calibration strategies and three cross-validated (leave-one-out) models for transforming analog video signals into thermal response

Strategy/model	FACTORY	A PRIORI	AD HOC	Predictors
n^a	56	96	11	
Linear regression model				GS ^b
RMSE ^c (°C)	0.82	4.25	0.26	
R^2 adj ^d	0.98	0.40	0.99	
Multiple regression model				GS, FPA ^e
RMSE (°C)	0.78	0.38	0.24	
R^2 adj	0.98	>0.99	>0.99	
Polynomial model (2 nd degree)				GS
RMSE (°C)	0.81	4.22	0.27	
R^2 adj	0.98	0.41	0.99	
Polynomial model (2 nd degree)				GS, FPA
RMSE (°C)	0.74	0.32	0.16	
R^2 adj	0.99	>0.99	>0.99	

Note: ^a Dataset size; ^b Grey-scale value (analog video signal); ^c Root mean square error; ^d Adjusted coefficient of determination; ^e The camera's focal-plane-array temperature.

Performance of three alternative calibration strategies used either default factory setting of camera, FACTORY, a priori calibration under controlled conditions, A PRIORI, or calibration performed at the time of measurement, AD HOC. Three cross-validated (leave-one-out) models transformed analog video signals using a TAU 320 camera with offset set to 4550 (14bit scale) and gain to 25 (8bit scale) into thermal response, using a blackbody radiation source (type/name) for providing target temperatures.

The advantage of an AD HOC approach is that site- and time-specific information may be included in the calibrations. It requires, however, that the conditions are stable during the period of calibration and measurements. Moreover, the approach is very time consuming, since many calibration points are necessary in order to avoid over-fitting. The alternative A PRIORI approach has the advantage of being performed in advance of measuring, thus saving crucial time during field operations. Further, the lack of time constraints enables more calibration points to be included, and the conditions during calibration are stable.

Including FPA temperature as a second predictor

reduced the RMSE and increased the R^2_{adj} in all models (with one exception; the polynomial model based on FACTORY calibration reduced RMSE, but R^2_{adj} increased from 0.98 to 0.99, Table 1). Including the FPA temperature in the calibration model implies that e.g. the A PRIORI approach may include a certain degree of site- and time-specific adaptation, by using the actual FPA temperature recorded during measurement when transforming the analog thermal video signal into temperature data.

The importance of considering the influence of the focal-plane-array temperature of the uncooled thermal camera on their thermal output was also emphasized by Nugent et al.^[14]. Jones et al.^[4] discussed the warming up of their camera electronics. During their experimental measurements they used a ‘constant temperature background’ measuring the lens cap to correct for this effect.

3.3 Showcases

3.3.1 Indoor proximal thermal measurement of phosphorus stress in barley

During the thermal measurements in the greenhouse, the roof ventilation window was open, allowing cold air (-2°C) to flow into the greenhouse (and warm air to flow out) in order to stabilize the in-house temperature at 13°C (Figure 5a). The incoming cold air influenced the ambient conditions in the greenhouse, inducing a thermal gradient during data acquisition (Figure 5b and 5c). We found a drop of about 3°C at the coldest spot in the middle part of the greenhouse, when analyzing the background reference in the experimental images. We also noticed a cooling effect on pots located next to a wall, as the cardboard backgrounds of these pots showed slightly lower (0.2°C) ambient temperatures than their nearest neighbor (Figure 5c). The influence of the ambient temperature gradient on the thermal measurements of the plant canopies is evident, as demonstrated for the plants in the control pots (Figure 5c). It was possible, however, by utilizing the measured background reference temperatures, to correct for the ambient temperature gradient (Figure 5c). After such correction the temperatures of the control plants ranged from 10.63°C to 11.43°C .

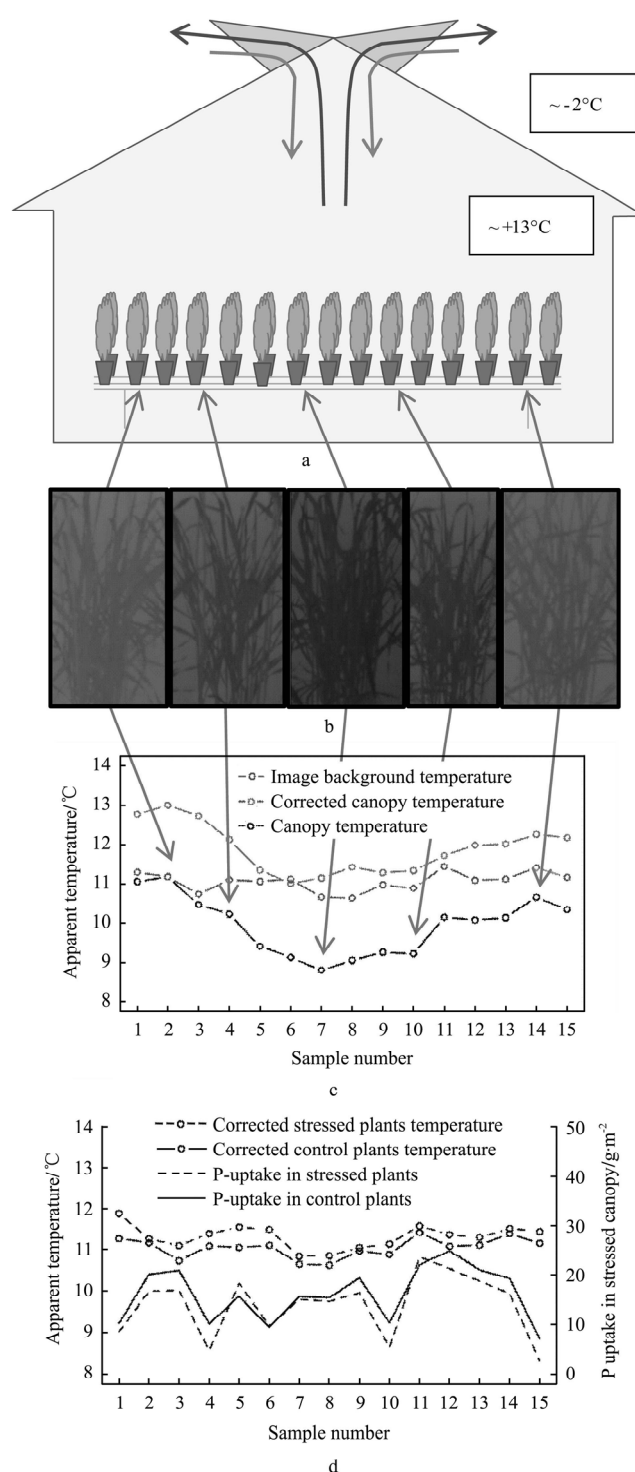


Figure 5 The experimental setup and selected results of the indoor phosphorus stress experiment including: (a) greenhouse outline with pots distribution and air flows, (b) sample raw thermal images of control plants at different locations in the greenhouse, (c) temperature measured on image background and control plants along with the corrected control plant temperatures, and (d) background corrected plant temperatures and plant above ground P-uptake in pots with P-deficit (P-stress) and in control pots

The plant available soil P content in the pots ranged from 28 to 267 mg/kg DM (including both P-limited and control pots). The corresponding above-ground plant P

contents ranged from 0.18 to 0.25 g P 100 g/DM, which equals 2.6 to 23.6 g P/m². When analyzing the thermal measurements of each pair of pots (i.e. two pots filled with the same soil, one with no P limitation of the growing barley plants, one with sub-optimum P content), we found in each pair, a temperature increase in the P-limited barley plants relative to the control (Figure 5d). However, the thermal response of the induced P stress was low, with an average difference between P-limited and control barley plants of only 0.27°C. The highest thermal difference was 0.61°C (Figure 5d).

In order to explore the relationship between measured temperature and plant P stress, we regressed the thermal recordings (corrected for background temperature) on the measured plant P content for a subset of samples with a soil P content below 215 mg/kg DM. The resulting model described 45% of the P variation in the analyzed subset. Although the model performance may appear poor, we found the results encouraging. It should be considered that in this example the covered temperature span was only 0.5°C, the number of points was low ($n=12$), and there was high soil variability, which also affected the plant moisture content.

Phosphorus deficiency in crops has to our knowledge not been investigated thermally. This may be due to the relatively low thermal effect it induces, compared to e.g. water deficiency^[4]. When measuring thermal differences of such a low magnitude as in this showcase, the effects of disturbing factors, such as background temperature gradients, may become highly important for the results, and should therefore be corrected for. Variation in greenhouse ambient temperature was also reported by Grant et al.^[27], who used a similar approach as that we used to correct for this effect.

In our showcase, P deficiency was the only factor that influenced plant growth, for which adjustment was made. Its relatively low impact on canopy temperature implies that in the presence of other growth stressors, i.e. water deficiency, under less controlled conditions the thermal effect of P stress may be hidden. Hence, the method of using thermal imaging to detect cereal P stress may be limited to use under controlled ambient environments, and with low variation in other growth factors.

3.3.2 Outdoor proximal thermal measurement of water stress in wheat

Two important challenges of using an analog thermal camera for proximal measurements under field conditions were identified in this showcase; variation related to the Bi-directional Distribution Function (BRDF^[26]) and atmospheric changes during measuring. Because the reflected solar irradiance is distributed in the canopy according to BRDF, the anisotropic distribution is also observed in the thermal images (Figure 6).

The data presented here show that the backscatter view angle (with the sun in front of the camera, Figure 6, right sub-plot) maximized the differences between stressed and non-stressed plants, reaching ca. 1°C). When the camera was placed at the frontscatter view angle (with the sun behind the camera, Figure 6, left sub-plot) or with the angle perpendicular to the principal plane (frontscatter-backscatter direction, Figure 6, top sub-plot) the corresponding differences were less than 0.5°C. These temperature variations may be attributed to the direction of the solar radiance distribution in the crop canopy, but also to the canopy architecture, as the amount of shadowed areas in the thermal image may greatly influence the results. The maximum difference between measurements at front- and backscatter view angles was 2.4°C (data not shown). This is similar to the finding of Jones et al.^[4], who observed 3°C higher temperatures of the sunlit part of grapevine plants than on the shaded side. There are most likely two reasons that can explain the good separation between plants of two different water status. One is reduced transpiration rate in leaves subject to water stress, due to the slower conductance (i.e.: [8]), whilst the second is difference in emissivity since drier plant have lower emissivity (ca. 0.95) than do well-watered ones (ca. 0.98)^[29].

The calculations performed in this experiment indicate that the view angle perpendicular to the principal plane approximates the average crop temperature best, but that the measurements collected at the backscatter view angle maximize the differences between stressed and non-stressed plants.

To reduce the BRDF effect on the thermal measurements we suggest measuring the target from

various azimuth angles and simply averaging the results. In practice, where multi-angular measurements are not available, care should be taken to retain a constant azimuth view angle towards the sun. A more accurate

correction of the BRDF effect on the reflective part of the apparent temperature would require collecting the irradiation data and applying a thermal BRDF model^[26].

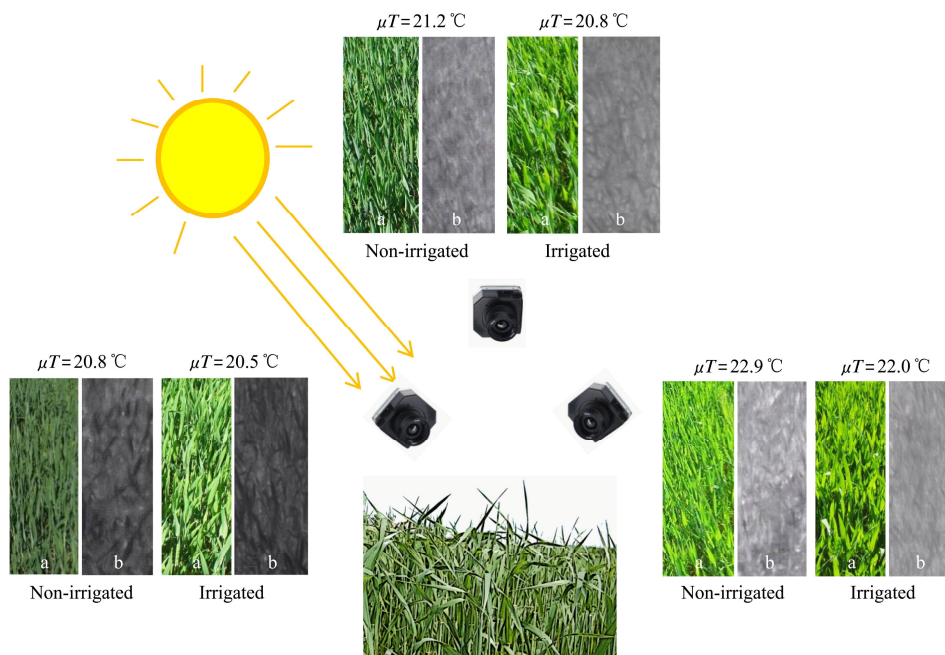


Figure 6 Angular dependency of view geometry relative to the position of the sun illustrated on: (a) visible (RGB) and (b) thermal images of an irrigated and a non-irrigated (stressed) wheat canopy. Average (i.e. across all pixels within the frame) image temperatures (μT) are indicated. The measurements were performed on 04.06.2013 16:03 CET at an ambient temperature of 25.5°C, with a wind speed of 3.8 m/s and illumination of 79.2 klux

Perhaps the biggest challenge in using a thermal camera outdoors is related to atmospheric changes during measurements. In this showcase, rapid weather fluctuations influenced the thermal readings (Figure 7). During a 90 minute measurement campaign we observed large fluctuations, and an increasing linear trend in the measured crop canopy temperatures, from around 20°C at the start to 22°C towards the end. The fluctuation around the trend was, as expected, related to the different crop water treatment (irrigated vs. non-irrigated), and the camera view angle, as discussed above. There were two major deviations from the trend, one at 15-20 minutes and one at around 50 minutes (Figure 7). The former episode was most likely a result of increased wind speed, as a wind gust of 6 m/s was recorded at the nearby weather station at about the same time as the canopy temperature was reduced by about 4.5°C from the current trend temperature of 20.8°C (Figure 7, left arrow). The slight mismatch in time may have been due to the distance to the weather station (200 m). The episode

around the 50th minute, when the canopy temperature dropped to 6.2°C below the current trend temperature of 21.3°C, may be explained by a 10% decrease in illumination over a period of 10 minutes (Figure 7, right arrow), related to the passing of a low cloud.

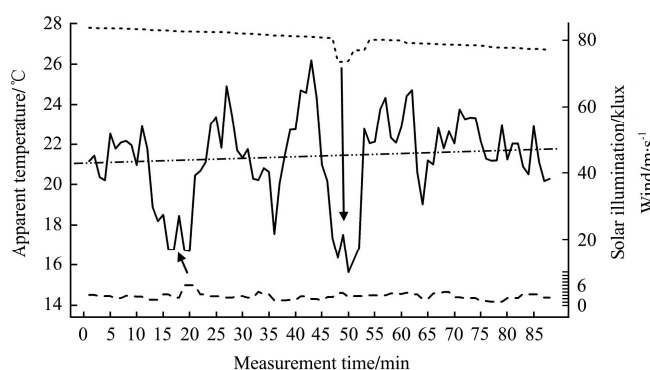


Figure 7 Apparent temperature of wheat canopies (solid line) measured proximally with a thermal camera during a 90 minute period (with overlaying linear trend, dash-dot line), covering both irrigated and non-irrigated plots, and wind speed (dashed line) and solar illumination (dotted line), as measured in a nearby weather station (200 m away). Two points of particular interest are indicated with arrows (see text for details)

The showcase experiment was large, so that the measuring time was relatively long, which implies that the risk of changes in the ambient conditions was high. Changes in the ambient conditions may, however, be corrected for by combining high quality weather data and modelling. As shown here, instant changes of atmospheric conditions related to wind gusts and changes in irradiance (illuminance) due to clouds and aerosols may significantly affect thermal measurements. The dependency of the apparent temperature on the atmospheric condition has been modeled by Leinonen et al.^[5] and is also well-described in [25] and [6]. Based on the experience obtained in the present showcase, it appears, however, that a one-minute resolution of the weather data is not sufficient to correct for changes in the ambient conditions, even when the weather conditions are relatively stable. We therefore suggest that outdoor proximal thermal canopy measurements require a one-second interval for atmospheric data acquisition at the measurement location, in order to obtain sufficient correction for disturbing factors. This may be considered as one of the limiting factors of simple, low-cost thermal data acquisition.

3.3.3 Outdoor remote thermal measurement of water stress in wheat

The same experiment was used in this showcase as in the previous one, but here the thermal measurements were taken remotely, from an altitude of 85 meters by means of a UAV (Figure 8a). The advantage of this setup was that a relatively large area may be covered by one image, thus avoiding the problem with changes in the ambient conditions during measuring. The challenge related to the Bi-directional Distribution Function (BRDF) remained, however, and the remote approach also introduced some additional challenges.

The raw data collected from the airborne platform ranged from 18.9°C to 24.2°C (Figure 8b). The displayed linear thermal trend appeared to be geometrically related to view angles along the principal plane of the solar illumination (related to the solar azimuth angle). The recorded temperatures were lower at backscatter and higher at frontscatter (Figure 8a), which was in accordance with the finding in the previous

showcase.

In order to correct for this tendency, we first tried to construct a single image-based trend (by finding the correlation between all pixel values and their position on the principal plane) to define the view-illumination anisotropy, but we did not obtain a satisfying fit. Instead, we defined two thermal gradients, and averaged them into a general trend (Figure 8b). By subtracting the (position specific) general trend from the thermal dataset, the observed thermal trend was corrected (Figure 8c). After such post-processing of the data it was possible to separate between stressed and non-stressed wheat plants, as the treatment related temperature difference was up to 2.5°C. The average difference between water stressed and non-stressed wheat canopies was 1.6°C. This distinct water status separation was obtained even though the water stress in the plants was not very pronounced, due to a high precipitation level in the preceding weeks.

The simple trend correction discussed above should be used before image rectification, which is typically used for view geometry correction of remotely obtained images^[30], to prevent thermal data distortion. An advantage of this simple method is that it requires less computation than a BRDF correction based on empirical or physical models^[26] and is therefore suitable for basic applications. Admittedly, the trend presented in Figure 8a was relatively easy to detect, since the controlled water treatments, which were mainly responsible for the thermal differences, were arranged in a perpendicular direction. If our approach is used on non-experimental fields we suggest finding a relative homogeneous part of the field, and looking for a trend in the direction of a principal plane there.

Airborne thermal imaging is probably the most challenging application. Typically, due to its larger field-of-view and larger pixel size, 'nadir-like' view angles are selected for airborne image acquisition. This slightly reduces the geometry induced image anisotropy, compared to the typical proximal sensing application. The image pixels acquired using wide-view lenses are typically highly anisotropic. Also, the airborne acquisition of imagery is influenced by the instability of

the platform, causing geometric image distortion, and influencing the viewing geometry, which must be corrected for in order to obtain sound results. Additionally, a vertical weather gradient may be present during measurements. Therefore, in a specific situation, the height of the measurement may also influence results. To correct for possible instant changes of the atmospheric conditions at the altitude of data acquisition, which were

not the case in our airborne experiment, we suggest including a set of airborne weather sensors to complement the ground weather station, in order to obtain advanced thermal measurement correction. That is especially important for low-altitude acquisition platforms, since the analyzed temperature variation is local and may be influenced by surrounding large objects and topography.

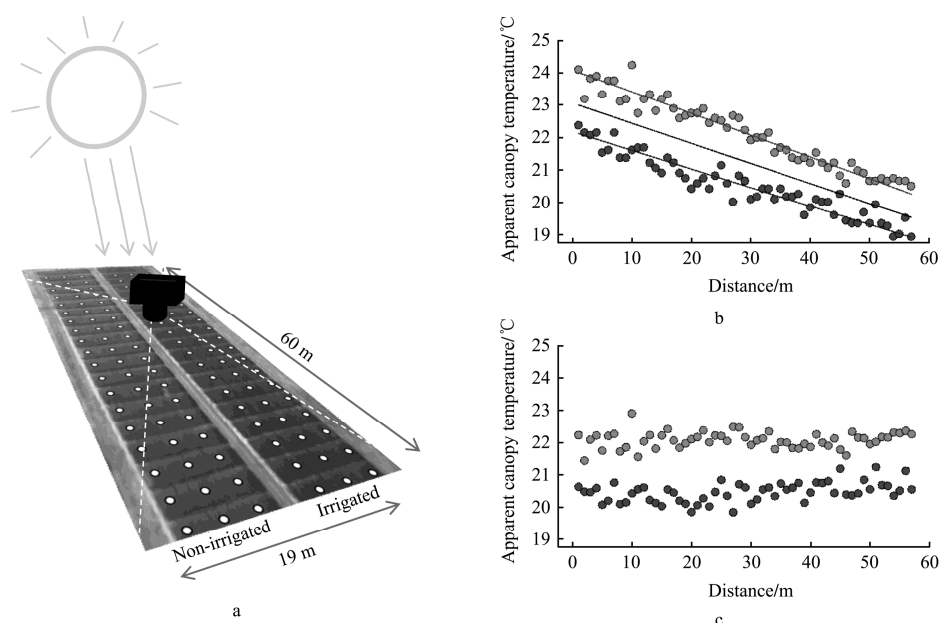


Figure 8 An outline of the airborne thermal image acquisition, showing (a) a single, raw thermal image taken from a height of 85 m at nadir view angle, but presented from another position here in order to illustrate the thermal gradient towards the sun. The dashed white lines indicate the camera position relative to the corners and center of the image, and the white points show the data sampling points. Further, (b) the apparent canopy temperatures are shown for irrigated (blue points) and non-irrigated (red points) plots, along with the corresponding trend lines (blue and red line, respectively, where the overall trend (i.e. the trend for all points in both treatments) is shown as a black line. In (c), the trend-corrected (using the overall trend for correction) canopy temperatures are shown for irrigated (blue points) and non-irrigated (red points) plots

4 Conclusions

- Changes in FPA temperature greatly affect thermal measurements obtained by an uncooled microbolometer thermal camera. Such a camera should be initialized and exposed to the measuring environment for at least 30-40 minutes before usage.
- Settings of gain and offset are crucial for the results, and the optimum combination depends on the temperature range of interest. Since camera performance is most sensitive to the offset setting, the optimum offset level should be identified first.
- Regression models may be well suited for transforming analog thermal video signals into

temperature data, if robust calibration data are available. We suggest creating a calibration data set under controlled conditions, and including information on FPA temperature as an independent variable in the model.

- It is possible to use thermal imaging to detect P-stressed barley plants under controlled conditions. The temperature difference between stressed and non-stressed plants is, however, so small that other factors that affect canopy temperature may easily over-shadow the P effect.
- Recording thermal measurements of a background reference is crucial in order to compensate for possible changes in ambient temperatures when

using thermal imaging in a greenhouse.

- To reduce the effect of bi-directional light distribution, which represents a challenge when using an analog thermal camera for proximal measurements under field conditions, the target should be measured from various azimuth angles, and the average temperature should be used for further analyses. Where multi-directional measurements are not available, care should be taken to retain a constant azimuth view angle towards the sun.
- Instant changes of atmospheric conditions related to wind gusts and changes in irradiance (illuminance), due to clouds and aerosols, may significantly affect proximal thermal measurements performed under field conditions. High quality weather data with a high time resolution (1 Hz) may then be needed for correction.
- Thermal measurements obtained from an UAV may, as proximal measurements, be affected of bi-directional light distribution, i.e. the solar azimuth angle. It is necessary to correct for trends resulting from this phenomenon. Corrected data may, however, provide a quality which allows the user to distinguish between stressed and non-stressed wheat plants.
- Advances in microbolometer camera technology reduce the cost and weight of the sensor which opens for a range of new applications in vegetation monitoring, including robotized portable measurement platforms. The remotely based plant stress detection method presented here, may be suitable for small agricultural and horticultural enterprises that require measurement systems with low investment cost. The method requires user skills, great care during measurements and appropriate correction of disturbing factors to obtain sufficient detection accuracy.

Acknowledgments

We thank A.Ø. Kristoffersen for allowing us to utilize the indoor pot experiment with phosphorus stress, and J. Jasper (Yara International ASA) for letting us perform

measurements at the field experiment at Hanninghof, Germany. The project was funded by the Research Council of Norway (Program: “Bionær”). H. Riley is gratefully acknowledged for critically reading the manuscript.

[References]

- [1] Jackson R D, Reginato R J, Idso S B. Wheat canopy temperature: A practical tool for evaluating water requirements. *Water Resour. Res.*, 1977; 13(3): 651–656. doi:10.1029/WR013i003p00651.
- [2] Cohen Y, Alchanatis V, Meron M, Saranga Y, Tsipris J. Estimation of leaf water potential by thermal imagery and spatial analysis. *Journal of Experimental Botany*, 2005; 56(417): 1843–52. doi:10.1093/jxb/eri174.
- [3] Thomson S J, Ouellet-Plamondon C M, DeFauw S L, Huang Y, Fisher D K, English P J. Potential and Challenges in Use of Thermal Imaging for Humid Region Irrigation System Management. *Journal of Agricultural Science*, 2012; 4(4): 103–116. doi:10.5539/jas.v4n4p103.
- [4] Jones H G, Stoll M, Santos T, de Sousa C, Chaves M M, Grant O M. Use of infrared thermography for monitoring stomatal closure in the field: application to grapevine. *Journal of Experimental Botany*, 2002; 53(378): 2249–2260. doi:10.1093/jxb/erf083.
- [5] Leinonen I, Grant O M, Tagliavia C P P, Chaves M M, Jones H G. Estimating stomatal conductance with thermal imagery. *Plant, Cell and Environment*, 2006; 29(8): 1508–1518. doi:10.1111/j.1365-3040.2006.01528.x.
- [6] Jones H G, Serraj R, Loveys B R, Xiong L, Wheaton A, Price A H. Thermal infrared imaging of crop canopies for the remote diagnosis and quantification of plant responses to water stress in the field. *Functional Plant Biology*, 2009; 36: 978–989. doi:10.1071/FP09123.
- [7] Munns R, James R, Sirault X R R, Furbank R T, Jones H G. New phenotyping methods for screening wheat and barley for beneficial responses to water deficit. *Journal of Experimental Botany*, 2010; 61(13): 3499–3507. doi:10.1093/jxb/erq199.
- [8] Vadivambal R, Jayas D S. Applications of Thermal Imaging in Agriculture and Food Industry—A Review. *Food and Bioprocess Technology*, 2010; 4(2): 186–199. doi:10.1007/s11947-010-0333-5.
- [9] Johnson J E, Shaw J A, Lawrence R, Nugent P W, Dobeck L M, Spangler L H. Long-wave infrared imaging of vegetation for detecting leaking CO₂ gas. *Journal of Applied Remote Sensing*, 2012; 6(1): 063612: 1–9. doi:10.1117/1.JRS.6.063612.
- [10] Bhan R K, Saxena R S, Jalwania C R, Lomash S K.

- Uncooled Infrared Microbolometer Arrays and their Characterisation Techniques. *Defence Science Journal*, 2009; 59(6): 580–589.
- [11] FLIR®. Does Tau or Quark, along with certain software, allow for thermography and temperature characterization? 2013. <http://www.flir.com/cvs/cores/knowledgebase/index.cfm?view=35837>. Accessed on [15.05.2013].
- [12] Machin G, Simpson R, Broussely M. Calibration and validation of thermal imagers. In: 9th International Conference on Quantitative InfraRed Thermography. July 2-5, 2008, Krakow, Poland. pp. 1–8.
- [13] Bower S M, Kou J, Saylor J R. A method for the temperature calibration of an infrared camera using water as a radiative source. *The Review of scientific instruments*, 2009; 80(9): 095–107. doi:10.1063/1.3213075.
- [14] Nugent P W, Shaw J A, Pust N J. Correcting for focal-plane-array temperature dependence in microbolometer infrared cameras lacking thermal stabilization. *Optical Engineering*, 2013; 52(6): 061304. doi:10.1117/1.OE.52.6.061304.
- [15] R Development Core Team. R: A language and environment for statistical computing. R Foundation for Statistical Computing, Vienna, Austria, 2008. ISBN 3-900051-07-0, <http://www.R-project.org>.
- [16] MathWorks Inc. MATLAB, version 7.7.0, 2008. MathWorks Inc., Natick, Massachusetts.
- [17] Gu C. Multidimensional Smoothing with Smoothing Splines. In *Smoothing and Regression: Approaches, Computation, and Application*, ed. M. G. Schimek. New York: Wiley, 2000.
- [18] Cleveland W S, Grosse E, Shyu W M. Local regression models. In: Chambers J M, Hastie T J (Ed.). *Statistical Models in S*. Wadsworth & Brooks/Cole, 1992. 317 p.
- [19] Bouguet J Y. Camera Calibration Toolbox for MATLAB, 2010. http://www.vision.caltech.edu/bouguetj/calib_doc/. Accessed on [10.06.2013].
- [20] Yahyanejad S, Misiorny J, Rinner B. Lens distortion correction for thermal cameras to improve aerial imaging with small-scale UAVs. In 2011 IEEE International Symposium on Robotic and Sensors Environments (ROSE). Montreal, QC, 17-18 Sept. 2011: IEEE. pp. 231–236. doi:10.1109/ROSE.2011.6058528
- [21] Luhmann T, Ohm J, Piechel J, Roelfs T. Geometric calibration of thermographic cameras. In: *International Archives of Photogrammetry, Remote Sensing and Spatial Information Sciences*, Vol. XXXVIII, Part 5, Commission V Symposium, Newcastle upon Tyne, UK, 2010. pp. 411–416.
- [22] Berni J A J, Member S, Zarco-Tejada P J, Suárez L, Fereres E. Thermal and Narrowband Multispectral Remote Sensing for Vegetation Monitoring From an Unmanned Aerial Vehicle. *IEEE Transactions on Geoscience and Remote Sensing*, 2009; 47(3): 722–738.
- [23] Vidas S, Lakemond R, Denman S, Fookes C, Sridharan S, Wark T. A Mask-Based Approach for the Geometric Calibration of Thermal-Infrared Cameras. *IEEE Transactions on Instrumentation and Measurement*, 2012; 61(6): 1625–1635. doi:10.1109/TIM.2012.2182851.
- [24] Electrophysics Corp. Understanding thermal camera image quality, 2013. http://www.electrophysics.com/e/dl-files/whitepapers_ph/WP-Ph-TIQ-v05.pdf. Accessed on [22.08.2013].
- [25] Jones H G, Schofield P. Thermal and other remote sensing of plant stress. *General and Applied Plant Physiology*, 2008; (34): 19–32.
- [26] Snyder W C. BRDF models to predict spectral reflectance and emissivity in the thermal infrared. *IEEE Transactions on Geoscience and Remote Sensing*, 1998; 36(1): 214–225. doi:10.1109/36.655331.
- [27] Grant O M, Chaves M M, Jones H G. Optimizing thermal imaging as a technique for detecting stomatal closure induced by drought stress under greenhouse conditions. *Physiologia Plantarum*, 2006; 127(3): 507–518. doi:10.1111/j.1399-3054.2006.00686.x.
- [28] Zia S, Spohrer K, Wenyong D, Spreer W, Xiongkui H, Muller J. Effect of Wind and Radiation on the Crop Water Stress Index Derived by Infrared Thermography. In *Conference on International Research on Food Security, Natural Resource Management and Rural Development Effect*, ETH Zurich. Zurich, September 14 – 16, 2010. pp. 3–6.
- [29] Olioso A, Sòria G, Sobrino J, Duchemin B. Evidence of Low Land Surface Thermal Infrared Emissivity in the Presence of Dry Vegetation. *IEEE Geoscience and Remote Sensing Letters*, 2007; 4(1): 112–116. doi: 10.1109/LGRS.2006.885857.
- [30] Demers M N. *Fundamentals of Geographic Information Systems*. John Wiley & Sons, 1997. 443 p.